




# Thermal activation in microwave-assisted magnetization switching and its effect on the switching behavior of granular media

Nobuaki Kikuchi <sup>1,2,\*</sup>, Katsunari Sato,<sup>1</sup> Satoshi Okamoto <sup>1,2</sup>, Osamu Kitakami <sup>1,2</sup>,  
Takehito Shimatsu,<sup>2,3,4</sup> and Hirofumi Suto<sup>5</sup>

<sup>1</sup>*Institute of Multidisciplinary Research for Advanced Materials, Tohoku University, Sendai 980-8577, Japan*

<sup>2</sup>*Center for Spintronics Research Network (CSRN), Tohoku University, Sendai 980-8577, Japan*

<sup>3</sup>*Frontier Research Institute for Interdisciplinary Sciences, Tohoku University, Sendai 980-8578, Japan*

<sup>4</sup>*Research Institute of Electrical Communication, Tohoku University, Sendai 980-8577, Japan*

<sup>5</sup>*Research Center for Magnetic and Spintronic Materials, National Institute for Materials Science (NIMS), Tsukuba 305-0047, Japan*



(Received 13 December 2020; revised 8 February 2022; accepted 8 February 2022; published 25 February 2022)

Microwave-assisted switching (MAS) has gathered fundamental interest and has been explored for magnetic recording since the switching field can be reduced by exciting magnetization with a microwave field in the GHz range. We theoretically study the effect of thermal activation in MAS and apply the developed analytical method to examine the result of MAS experiments on CoCrPt-SiO<sub>2</sub> granular media. The effective energy barrier height for magnetization switching under a microwave field is calculated from the Landau-Lifshitz-Gilbert equation. The calculated energy barrier shows that the thermal activation process plays a crucial role in MAS and modifies the dependences of the switching field on the microwave frequency and amplitude. The switching field decreases with increasing the microwave frequency up to the critical frequency, at which point the switching field abruptly increases. Thermal activation significantly increases the critical frequency and makes the slope of the frequency dependence of the switching field gradual. The maximum assistance effect increases with increasing the microwave field amplitude and is almost independent of the thermal activation. The analytical method quantitatively explains the gradual microwave frequency dependence and high critical frequency observed in MAS experiments on granular media. These results indicate the importance of thermal activation to optimize MAS behavior for practical use.

DOI: [10.1103/PhysRevB.105.054430](https://doi.org/10.1103/PhysRevB.105.054430)

## I. INTRODUCTION

Magnetization dynamics in a microwave field has been studied for decades. Ferromagnetic resonance (FMR) is one of the most intensively studied topics, in which magnetization absorbs microwave energy resonantly and precesses around the effective field. Microwave field amplitude is negligibly small compared with the effective field in general FMR experiments. By increasing the microwave field amplitude further up to of the order of  $10^{-2}$  of the anisotropy field, microwave helps magnetization to climb up its potential well and overcome the energy barrier for irreversible switching with a reduced external field. The phenomenon is called microwave-assisted magnetization switching (MAS). MAS has attracted wide interest as a key technology for microwave-assisted microwave recording (MAMR) [1–4], which allows us to employ magnetic media with higher anisotropy and realize hard disk drives (HDDs) with higher capacity.

Theoretical studies on MAS have shown that microwave frequency dependences of the assistance effect can be explained based on the Landau-Lifshitz-Gilbert (LLG) equation in a rotating frame [5–12]. In the rotating frame synchronized with the rotating microwave field of  $f_{rf}$  in frequency,

the effect of microwave field frequency can be translated to a fictitious field with a magnitude of  $2\pi f_{rf}/\gamma$  along the rotation axis, where  $\gamma$  is the gyromagnetic ratio. Therefore, the irreversible switching field of a single spin under a microwave field can be described by the Stoner-Wohlfarth model considering a sum of the external dc field, the microwave field, and the fictitious field [6–12]. The theories predict that the assistance effect is proportional to the frequency with the proportional factor of  $-2\pi/\gamma$ , but almost insensitive to microwave field amplitude. Another key feature of MAS is the critical frequency, at which the assistance effect suddenly vanishes. The quantitative expression of the critical frequency has been derived as a function of microwave field amplitude based on the LLG equation in a rotating frame [10].

Experimental studies on MAS have been carried out extensively on both nanostructured magnets [13–18] and granular magnetic recording media [19–27]. Experiments on nanostructured magnets have shown good agreement with the theoretical prediction, showing the linear decrease of the switching field with the slope of  $-2\pi/\gamma$  and the sudden vanishment of the assistance effect at the critical frequency [14–18]. On the contrary, experimentally obtained results in granular media differ from the theories in terms of the smaller assistance effect and the unclear critical frequency [19–27]. From a practical point of view, it is important to understand

\*nobuaki.kikuchi.d6@tohoku.ac.jp

MAS behavior in granular media, since the media are supposed to be employed in HDDs based on MAMR [4].

We recently pointed out that the assistance effect had been underestimated due to the experimental procedure employed in the previous studies [27], in which microwave fields were applied as periodic pulses with nanoseconds duration to prevent damaging samples [14–26]. A large difference exists in the timescale between microwave and dc fields, making it difficult to analyze the assistance effect properly. To eliminate such ambiguousness due to the timescale difference, we have carried out MAS experiments on a CoCrPt-SiO<sub>2</sub> granular medium by applying a microwave field as continuous waves [27]. The experiments have revealed that the coercivity of the granular media decreases almost linearly with increasing microwave frequency, and the slope of frequency dependence increases with the microwave field amplitude. Such microwave field amplitude dependent behavior is inconsistent with the theories and experimental results on nanostructured magnets, indicating that MAS behavior in granular media has to be understood based on a different theory. One of the essential differences between granular media and nanostructured magnets is their volume. Magnetization reversal of granular media is strongly influenced by thermal activation because of its small grain size of sub-10 nm. Another important difference in MAS experiments is the ratio of microwave field amplitude and the anisotropy field. The ratio tends to be smaller for granular media, because of its high-anisotropy field reaching almost 2 T.

Suto *et al.* reported that the effective energy barrier height under a microwave field can be calculated based on the LLG equation in the rotating frame [9]. The effective energy barrier height shows complicated microwave field frequency and dc field dependences, suggesting that the thermal activation process strongly influences MAS behavior. However, in previous experimental studies, almost no attention has been paid to the effect of the thermal activation process on frequency dependences. Moreover, there was no discussion about the effect of microwave field amplitude, which is an important issue for both fundamental and practical points of view.

In this study, we investigate switching behavior under the microwave field, particularly focusing on thermal activation. The effective energy barrier height for MAS is calculated based on the LLG equation in a rotating frame for various microwave field amplitudes. The evaluated effective energy barrier height gives the relation between switching probability and the condition of applied dc and microwave fields. Numerical simulations based on the LLG equation were performed to evaluate switching behavior at finite temperature to investigate the validity of the analytical calculation. MAS experiments were carried out on CoCrPt-SiO<sub>2</sub> with continuous fields with varied microwave field amplitude. The obtained experimental dependences of the switching field on microwave amplitude and frequency are quantitatively explained by the theory.

## II. EFFECTIVE ENERGY BARRIER FOR MAGNETIZATION SWITCHING IN MICROWAVE FIELD

In this section, we discuss the effective energy barrier height  $\Delta\varepsilon$  for magnetization switching in a microwave field based on the LLG equation in a rotating frame [9], which

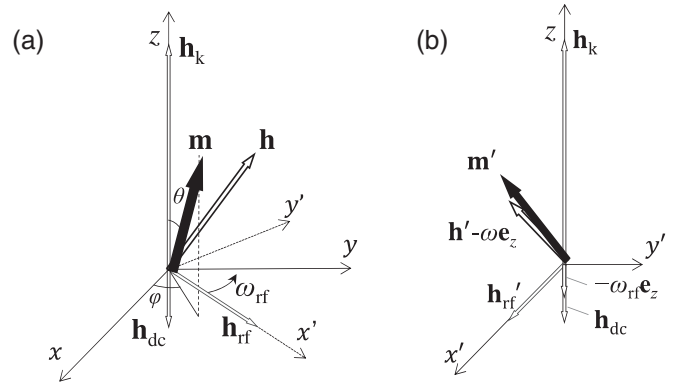


FIG. 1. Definition of magnetization and fields in (a) stationary frame and (b) rotating reference frame.

is often employed to discuss magnetization behavior in microwave fields. Based on the LLG equation in a rotating frame, magnetization gains or dissipates energy during one precession cycle depending on the condition of magnetization and applied fields, while magnetization always dissipates energy in a laboratory frame. Therefore, we introduced the effective energy  $\varepsilon$  to evaluate the stability of magnetization and to discuss the thermal activation process in MAS. Magnetization overcomes the finite energy barrier under thermal activation, and its switching probability is described using the Néel-Arrhenius formula as a function of time and energy barrier height  $\Delta E$  in the unit of temperature multiplied by the Boltzmann constant,  $k_B T$ . The relaxation time  $\tau$  can be expressed as  $\tau = f_0^{-1} \exp(-\Delta E)$  following the formula. Therefore, switching behavior under thermal activation in MAS can be evaluated in a wide time range scale by calculating  $\Delta\varepsilon$  as functions of microwave frequency and applied dc field. First, we review the calculation procedure and phase portraits of the effective energy  $\varepsilon$ , following Suto's procedure. Here, we assume a single spin  $\mathbf{M}$  with the saturation magnetization  $M_s$  and the uniaxial anisotropy  $K_u$ , corresponding to the anisotropy field  $H_k = 2M_s/K_u$ . By using the normalized magnetization  $\mathbf{m} = \mathbf{M}/M_s$ , the normalized time  $\tau = t(\gamma H_k)$ , and the normalized field  $\mathbf{h} = \mathbf{H}/H_k$ , the LLG equation that a single spin follows is described as

$$\frac{d\mathbf{m}}{d\tau} = -\mathbf{m} \times \mathbf{h} + \alpha \mathbf{m} \times \frac{d\mathbf{m}}{d\tau}, \quad (1)$$

where  $\alpha$  and  $\gamma$  are the Gilbert damping and the gyromagnetic ratio. Here we consider the system configuration illustrated in Fig. 1(a). The polar angle and the azimuthal angle of  $\mathbf{m}$  are defined as  $\theta$  and  $\varphi$ , and  $\mathbf{h}_k = m_z \mathbf{e}_z$  represents the normalized anisotropy field. The easy axis of the spin is along the  $z$  axis, and initial magnetization is set to the  $+z$  direction.  $\mathbf{h}_{dc}$  and  $\mathbf{h}_{rf}$  represent an external static field along the  $z$  axis and a rotating microwave field in the  $x$ - $y$  plane, respectively.  $\mathbf{h}_{rf}$  is rotated counterclockwise with the angular frequency of  $\omega_{rf}$ , so that  $\mathbf{h}_{rf}$  can excite magnetization pointing in the  $+z$  direction. Notice that the amplitude of a linearly polarized field should be halved if one compares with a circularly polarized field since a linearly polarized one is a superposition of clockwise and counterclockwise circularly polarized fields. The field  $\mathbf{h}$  in Eq. (1) expresses the sum of all those fields

( $\mathbf{h} = \mathbf{h}_{\text{dc}} + \mathbf{h}_{\text{k}} + \mathbf{h}_{\text{rf}}$ ). By employing a rotating frame rotating with  $\omega_{\text{rf}}$  around the  $z$  axis, the system is converted as shown in Fig. 1(b). In the rotating frame,  $\mathbf{h}_{\text{rf}}$  can be treated as a static field along the  $x'$  axis by choosing the initial phase properly. A fictitious field  $\omega_{\text{rf}}$  along the  $z$  axis appears. Equation (1) can be transformed in the rotating frame as

$$\frac{d\mathbf{m}'}{d\tau} = -\mathbf{m}' \times (\mathbf{h}' - \omega_{\text{rf}}\mathbf{e}_z) - \alpha \mathbf{m}' \times (\mathbf{m}' \times \mathbf{h}'), \quad (2)$$

where  $\mathbf{m}'$ ,  $\mathbf{h}'$ , and  $\mathbf{e}_z$  are the magnetization and the field in the rotating frame, and the unit vector along the  $z$  axis, respectively. Here, it is assumed that  $\alpha$  is small and its quadratic term is negligible. Equation (2) can be rewritten as

$$\begin{aligned} \frac{d\mathbf{m}'}{d\tau} = & -\mathbf{m}' \times (\mathbf{h}' - \omega_{\text{rf}}\mathbf{e}_z) - \alpha \mathbf{m}' \times [\mathbf{m}' \times (\mathbf{h}' - \omega_{\text{rf}}\mathbf{e}_z)] \\ & - \alpha \omega_{\text{rf}}\mathbf{m}' \times (\mathbf{m}' \times \mathbf{e}_z), \end{aligned} \quad (3)$$

to have the field terms in the precession and the damping terms have the same form of  $\mathbf{h}' - \omega_{\text{rf}}\mathbf{e}_z$ . The newly appeared third term on the right-hand side of Eq. (3) expresses the torque aligning magnetization along the  $z$  axis, which always works to prevent magnetization from switching. The magnitude of the term is proportional to  $\omega_{\text{rf}}$ . Equation (3) has a form similar to the case of the spin torque, and it is applicable for deriving the effective energy  $\varepsilon$  for magnetization switching in a microwave field following the procedure used in the spin-torque switching [28]. In order to define  $\varepsilon$ , the potential energy  $\tilde{g}$  in the rotating frame is defined as

$$\tilde{g} = -\mathbf{m} \cdot (\mathbf{h}_{\text{dc}} + \mathbf{h}_{\text{rf}} - \omega_{\text{rf}}\mathbf{e}_z) - \frac{1}{2}m_z^2. \quad (4)$$

By using the potential energy  $\tilde{g}$ , the effective energy  $\varepsilon(\tilde{g})$  representing the required energy to move magnetization from one reference energy contour  $C(\tilde{g}_0)$  to another contour  $C(\tilde{g})$  is defined as

$$\varepsilon(\tilde{g}) = \int_{\tilde{g}_0}^{\tilde{g}} \frac{\mathcal{W}_{\text{dis}}(\tilde{g}') + \mathcal{W}_{\text{rf}}(\tilde{g}')}{\mathcal{W}_{\text{dis}}(\tilde{g}')} d\tilde{g}'. \quad (5)$$

$\mathcal{W}_{\text{dis}}(\tilde{g}')$  and  $\mathcal{W}_{\text{rf}}(\tilde{g}')$  are the line integrals defined as  $-\alpha \oint_{C(\tilde{g}')} [\mathbf{m}' \times (\mathbf{h}' - \omega_{\text{rf}}\mathbf{e}_z)] \cdot d\mathbf{m}'$  and  $-\alpha \oint_{C(\tilde{g}')} (\mathbf{m}' \times \omega_{\text{rf}}\mathbf{e}_z) \cdot d\mathbf{m}'$ , respectively.  $\mathcal{W}_{\text{dis}}(\tilde{g}')$  gives a value proportional to the change in  $\tilde{g}$  due to energy dissipation during one precession motion along the contour  $C(\tilde{g}')$ , while  $\mathcal{W}_{\text{rf}}(\tilde{g}')$  gives the change in  $\tilde{g}$  caused by the microwave field. Those two terms correspond to energy dissipation or gain by the second and the third terms in the right-hand side of Eq. (3). Here, we chose the reference value  $\tilde{g}_0$  as the maximum value of  $\tilde{g}$ . For the case of zero fields, the relations  $\varepsilon(\tilde{g}) = \tilde{g}_0 - \tilde{g}$  hold, and the energy barrier height  $\Delta\varepsilon = 0.5$  can be deduced from Eq. (4). More detailed calculation procedures have been presented in previous works [8,9].

The potential energy  $\tilde{g}$  has either two or four fixed points depending on the field parameters. In the case of two fixed points, the fixed points are global minimum and maximum. Saddle point and local minimum additionally appear in the case of four fixed points. Those fixed points in the rotating frame represent rigidly rotating magnetization with excitation frequency in the laboratory frame. Attractive and repulsive limit cycles appear as a periodic motion on a closed path in

the rotating frame. Those limit cycles work as pseudostable and pseudounstable fixed points in the phase portrait of  $\varepsilon$  [9]. The phase portrait of  $\varepsilon$  can be categorized by the number and stability of fixed points and the presence of attractive/repulsive limit cycles [5,9,29]. The detailed location of the fixed points and limit cycles are given in the  $\theta$ - $\varphi$  plane in Ref. [9]. For a qualitative understanding of the effect of the spin-torque term, it is helpful to categorize the contour of  $\tilde{g}$  into four types related with the location of fixed points. The first three are contours surrounding the local minimum, the maximum, and the global minimum. These three show different contributions to  $\varepsilon$  and  $\omega_{\text{rf}}$  dependence. The other one is the contour passing the saddle point. In Figs. 2(a)–2(c), a contour map of the free energy  $\tilde{g}$  is plotted on the surface of a sphere for  $h_{\text{dc}} + \omega_{\text{rf}} = 0.4$  and  $h_{\text{rf}} = 0.1$ . Typical contour lines for the case of surrounding (a) local minimum, (b) maximum, and (c) global minimum are shown with bold lines in each figure. The solid and dashed arrows on those contour lines in the figures indicate the direction of the second (damping) term and the third (spin-torque) term of the right-hand side of Eq. (3). Note that the length of the arrows does not represent the amplitude of the terms to adjust visibility. For the case of Fig. 2(a), all the arrows are pointing inside of the contour, so that magnetization dissipates energy during one precession motion along the contour independent of microwave frequency  $\omega_{\text{rf}}$ . When magnetization precesses on the contour surrounding the maximum as shown in Fig. 2(b), the arrows of the spin-torque term on the upper half of the contour point outside the contour the same as the damping term, corresponding to energy dissipation during precession. On the contrary, the arrows of the spin-torque term on the lower half of the contour point inside the contour, meaning that the magnetization gains energy moving on the path. Because the spin-torque term is proportional to  $\mathbf{m}' \times \mathbf{e}_z$ , the effect of the spin-torque term is larger on the lower part of the contour than on the upper part. Therefore, the magnetization always gains energy by the spin-torque term during one precession on the contour line surrounding the maximum. Since the gain is proportional to the microwave frequency  $\omega_{\text{rf}}$ , the gain due to the spin-torque term and the dissipation due to the damping term may balance under a certain value of  $\omega_{\text{rf}}$ . At the balanced condition,  $\varepsilon$  takes local minimum, which is the attractive limit cycle. However, since too low (high)  $\omega_{\text{rf}}$  makes the damping (spin-torque) term dominant on all the contours, the attractive limit cycle appears in a rather narrow window of conditions. For the case of contour surrounding the global minimum shown in Fig. 2(c), the damping term points to the global minimum located close to the  $-z$  direction, while the spin-torque term directs the  $+z$  direction. These two terms are almost antiparallel, so that the total gain/dissipation during precession can be understood as the competition of the strength of these two terms. The contour on which the two terms are balanced corresponds to the repulsive limit cycle and works as the effective energy barrier in MAS.

Figure 3 shows the complete phase diagram of the phase portrait of the effective energy  $\varepsilon$  in the  $\omega_{\text{rf}}$ - $h_{\text{dc}}$  plane for  $h_{\text{rf}} = 0.025$ . The diagram consists of eight different phases labeled using the string notations, which express the stability and presence of the fixed points [5,9,29]. The characters in the string notation express the stable fixed point ( $s$ ), unstable fixed point ( $u$ ), saddle point ( $d$ ), repulsive limit cycle ( $r$ ), and

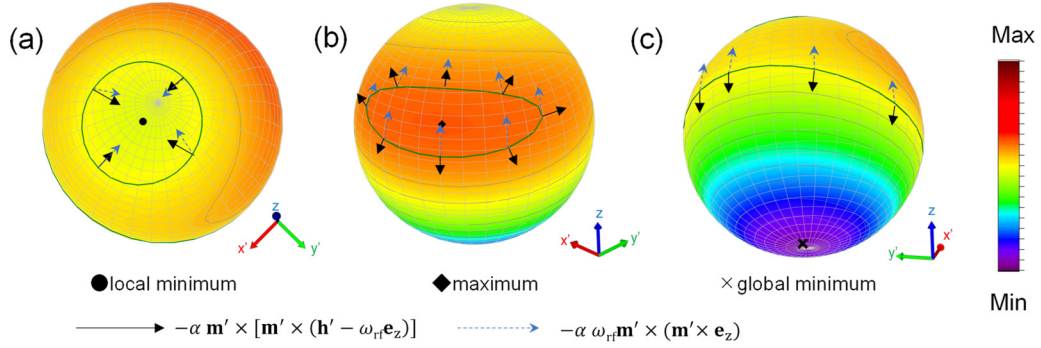


FIG. 2. Contour plot of free energy  $\tilde{g}$  distribution on the unit sphere for  $h_{dc} + h_{\omega} = 0.4$  and  $h_{rf} = 0.1$ . Contours surrounding (a) local minimum, (b) maximum, and (c) global minimum are shown as bold lines. The symbols in the plots indicate the location of the fixed points. The solid and dashed arrows indicate the direction of damping term and the spin-torque term, respectively. The length of the arrows does not represent the amplitude of those terms.

attractive (a) limit cycle. The light gray colored region ( $s|u$ ) corresponds to the condition at which deterministic switching occurs. Figure 4 shows typical phase portraits and the definition of effective energy barrier height  $\Delta\varepsilon$  for each string notation shown in Fig. 3. The symbols in the figure indicate the fixed points and the limit cycles, and their stability is represented by filled and unfilled symbols for stable and unstable, respectively. The scale bar in Fig. 4(a) corresponds to 0.1 for both  $\varepsilon$  and  $\tilde{g}$  axes of each figure except Fig. 4(c), which is enlarged for visibility. Figure 4(a) shows the phase portrait of ( $s|ud|s$ ) for  $h_{dc} = 0.2$  and  $\omega_{rf} = 0.1$ . The phase has four fixed points and no limit cycle. The global and the local minima are stable, and they are doubly connected to the unstable maximum at the saddle point. The arrow points to the global minimum location, which is located out of the plot range. The effective energy barrier height  $\Delta\varepsilon$  for ( $s|ud|s$ ) is defined as the difference of  $\varepsilon$  between at the saddle point ( $\varepsilon_{saddle}$ ) and the local minimum ( $\varepsilon_{l\_min}$ ). By increasing

the dc field to  $h_{dc} = 0.9$  while the frequency is constant at  $\omega_{rf} = 0.1$ , the stable global minimum and the unstable local minimum are directly connected without barrier, as shown in Fig. 4(b), which corresponds to the case of deterministic switching. Figure 4(c) shows the phase portrait for ( $sr|au$ ) for  $h_{dc} = 0.71$  and  $\omega_{rf} = 0.18$ , which appears in a rather narrow region around the critical frequency. Note that the vertical axis for  $\varepsilon$  and the lateral axis for  $\tilde{g}$  are magnified 100 times and 10 times, respectively, for visibility. In the ( $sr|au$ ) portrait, the stable global minimum surrounded by the repulsive limit cycle and the unstable maximum surrounded by the attractive limit cycle are connected without a saddle point. The limit cycles act as pseudounstable and stable points in  $\varepsilon$ , and  $\Delta\varepsilon$  is defined by the effective energy difference between the repulsive cycle ( $\varepsilon_{rep.}$ ) and the attractive limit cycle ( $\varepsilon_{att.}$ ). Figure 4(d) shows the phase portrait of ( $sr|ud|s$ ) for  $h_{dc} = 0.2$  and  $\omega_{rf} = 0.4$ .

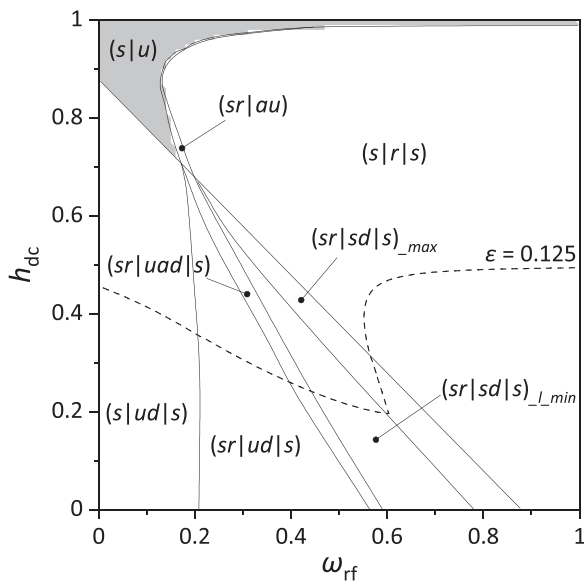


FIG. 3. Phase diagram of the phase portrait of the effective energy  $\varepsilon$  in the  $\omega_{rf}$ - $h_{dc}$  plane for  $h_{rf} = 0.025$ . The string notation represents the stability and presence of fixed points and limit cycles.

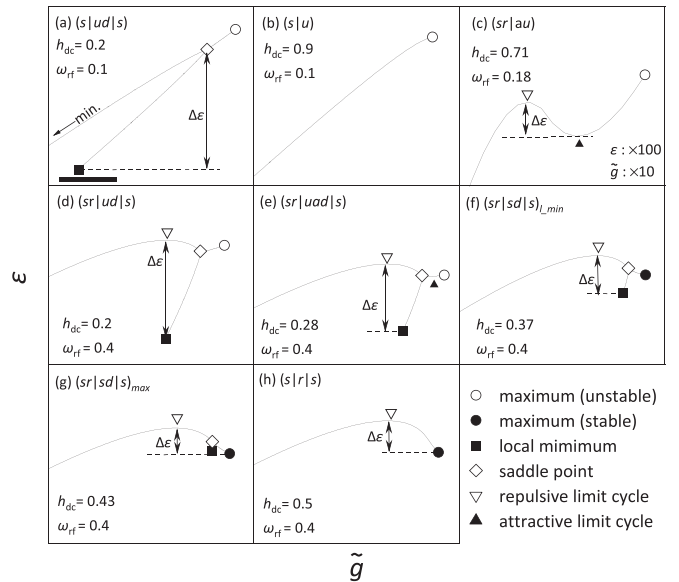


FIG. 4. Phase portrait of the energy barrier height  $\Delta\varepsilon$  as a function of potential energy  $\tilde{g}$  for (a) ( $s|ud|s$ ), (b) ( $s|u$ ), (c) ( $sr|au$ ), (d) ( $sr|ud|s$ ), (e) ( $sr|uad|s$ ), (f) ( $sr|sd|s$ ) <sub>$l\_min$</sub> , (g) ( $sr|sd|s$ ) <sub>$max$</sub> , and (h) ( $s|r|s$ ). Symbols in the phase portrait indicate fixed points and limit cycles with their stability.

TABLE I. Presence of saddle point, repulsive limit cycle, attractive limit cycles, stable maximum, and the definition of  $\Delta\varepsilon$  for each string notation.

String notations	Saddle	Repulsive	Attractive	Stable max	$\varepsilon_{l_{\min}} < \varepsilon_{\max}$	$\Delta\varepsilon$
$(s u)$						0
$(sr au)$		X	X			$\varepsilon_{\text{rep}} - \varepsilon_{\text{att}}$
$(s ud s)$	X					$\varepsilon_{\text{saddle}} - \varepsilon_{l_{\min}}$
$(sr ud s)$	X	X				$\varepsilon_{\text{rep}} - \varepsilon_{l_{\min}}$
$(sr uad s)$	X	X	X			$\varepsilon_{\text{rep}} - \varepsilon_{l_{\min}}$
$(sr sd s)_{l_{\min}}$	X	X		X	X	$\varepsilon_{\text{rep}} - \varepsilon_{l_{\min}}$
$(sr sd s)_{\max}$	X	X		X		$\varepsilon_{\text{rep}} - \varepsilon_{\max}$
$(s r s)$		X		X		$\varepsilon_{\text{rep}} - \varepsilon_{\max}$

In this portrait, a repulsive limit cycle appears between the saddle point and the global minimum, so that  $\Delta\varepsilon$  is given as  $\Delta\varepsilon = \varepsilon_{\text{rep}} - \varepsilon_{l_{\min}}$ . By increasing the dc field to  $h_{\text{dc}} = 0.28$ , the  $(sr|uad|s)$  portrait appears, in which an attractive limit cycle appears between the saddle point and the maximum [Fig. 4(e)]. The transition from  $(sr|ud|s)$  to  $(sr|uad|s)$  does not give any change to the definition of  $\Delta\varepsilon$ . By increasing the dc field, the  $(sr|sd|s)$  phase portrait appears, in which the effective energy at the maximum ( $\varepsilon_{\max}$ ) becomes smaller than  $\varepsilon_{\text{saddle}}$ . In the  $(sr|sd|s)$  phase portrait, two stable fixed points are connected to the saddle point, which is separated from the global minimum by the repulsive limit cycle. As shown in Figs. 4(f) and 4(g), two situations can be distinguished for the phase portraits expressed by the string notation  $(sr|sd|s)$ . One is the case for  $\varepsilon_{l_{\min}} < \varepsilon_{\max}$  as shown in Fig. 4(f), so that  $\Delta\varepsilon$  is given by  $\varepsilon_{\text{rep}} - \varepsilon_{l_{\min}}$ , the same as the  $(sr|ud|s)$  and  $(sr|uad|s)$  phase portrait. This phase portrait is named  $(sr|sd|s)_{l_{\min}}$ . By increasing the dc field further,  $\varepsilon_{\max}$  becomes smaller than  $\varepsilon_{l_{\min}}$ , so that  $\Delta\varepsilon$  is defined by  $\varepsilon_{\text{rep}} - \varepsilon_{\max}$  as shown in Fig. 4(g). The phase portrait is named  $(sr|sd|s)_{\max}$ . In Ref. [9], the activation process in the  $(sr|sd|s)$  portraits was treated as sequential double barriers and  $\Delta\varepsilon$  was given by the larger one of those two barriers. For example, in the case of  $(sr|sd|s)_{l_{\min}}$  shown in Fig. 4(f), two-step sequential activation processes are assumed; the first one is from local minimum to maximum over the saddle point. The second one is from the maximum to the global minimum over the repulsive limit cycle. However, the magnetization cannot stay at the maximum and should be back to the local minimum because of its shorter relaxation time due to the lower-energy barrier height. Therefore, it is more appropriate to assume a direct activation process from the local minimum to the global minimum over the repulsive limit cycle for  $(sr|sd|s)_{l_{\min}}$ . The treatment of the double barrier process for  $(sr|sd|s)_{\max}$  and  $(sr|sd|s)_{l_{\min}}$  is the main difference from the results of Ref. [9], which gives a significant impact on the critical frequency of MAS under finite temperature as discussed below. In Table I, the presence and stability of the fixed points and limit cycles are summarized for all string notations that appeared in Fig. 3. The definition of the  $\Delta\varepsilon$  for each string notation is also presented.

In Fig. 3, the contour line for  $\Delta\varepsilon = 0.125$  is shown as a dashed line. In the  $(s|ud|s)$  phase portrait, the contour line is concave downward and has a negative slope. By increasing  $\omega_{\text{rf}}$ , the concavity changes from downward to upward at the border between  $(s|ud|s)$  and  $(sr|ud|s)$ . At this border, the

repulsive limit cycle appears, and the definition of  $\Delta\varepsilon$  changes from  $\varepsilon_{\min} - \varepsilon_{l_{\min}}$  to  $\varepsilon_{\text{rep}} - \varepsilon_{l_{\min}}$ . The contour line shows a very sharp kink at the boundary between  $(sr|sd|s)_{l_{\min}}$  and  $(sr|sd|s)_{\max}$ , and the value of  $h_{\text{dc}}$  steeply increases while  $\omega_{\text{rf}}$  is almost unchanged and then enters into the  $(s|r|s)$  phase. In the  $(s|r|s)$  phase, the contour line bends and shows an almost constant value in the high- $\omega_{\text{rf}}$  region. The constant value in the high- $\omega_{\text{rf}}$  region is almost equal to the value of  $\Delta\varepsilon$  without the microwave field, indicating the microwave field loses its assistance effect in that frequency range. Since the contour line corresponds to the switching field under certain thermal activation conditions, the sharp kink at the boundary between  $(sr|sd|s)_{l_{\min}}$  and  $(sr|sd|s)_{\max}$  represents the critical frequency. In other words, the condition  $\varepsilon_{\max} = \varepsilon_{l_{\min}}$  gives the critical frequency in the presence of thermal activation. The sharp transition occurs because the third term of the right-hand side of Eq. (3) becomes dominant in the  $(sr|sd|s)_{\max}$  phase and the increase of  $\omega_{\text{rf}}$  prevents magnetization switching. Notice that the dip is located at  $\omega \sim 0.60$  for  $\Delta\varepsilon = 0.125$ . The frequency is quite large compared to the critical frequency at zero temperature  $\omega_c \sim 0.16$ , which is given as the frequency at the vertex of the dip of the  $(s|u)$  region. The result predicts that the experimentally observable critical frequency is strongly influenced by thermal activation and therefore depends on measurement conditions. Here, we define the critical frequency as a function of the effective energy barrier height,  $\omega_c(\Delta\varepsilon)$ . The critical frequency at zero temperature is given by  $\omega_c(0)$ .

In Figs. 5(a)–5(c), the effective energy barrier height  $\Delta\varepsilon$  for irreversible switching is shown as color maps in the  $\omega_{\text{rf}} - h_{\text{dc}}$  plane for  $h_{\text{rf}} =$  (a)  $6.25 \times 10^{-3}$ , (b)  $2.5 \times 10^{-2}$ , and (c) 0.1. The black regions at the top left in the maps correspond to the  $(s|u)$  phase portrait, at which deterministic switching occurs. The contour lines are plotted with a step of 0.05. The shape of the  $\Delta\varepsilon$  profiles strongly depends on  $h_{\text{rf}}$ . The slope of the contour lines in the low-frequency region becomes steeper by increasing  $h_{\text{rf}}$ . However, notice that the slopes of all contour lines are more gradual than  $-1$ , which is the slope predicted by the theories at zero temperature. Those results indicate that the frequency dependence of the switching field under finite temperature should always be more gradual than that in theories. The value of  $\omega_c(\Delta\varepsilon)$  increases along the boundary between  $(sr|sd|s)_{l_{\min}}$  and  $(sr|sd|s)_{\max}$  by increasing  $\Delta\varepsilon$ . In Figs. 5(d)–5(f),  $\Delta\varepsilon$  is plotted as a function of  $h_{\text{dc}}$  for (d)  $h_{\text{rf}} = 6.25 \times 10^{-3}$ , (e)  $2.5 \times 10^{-2}$ , and (f) 0.1. The profiles with a microwave field of  $\omega_{\text{rf}} = 0-0.8$  are

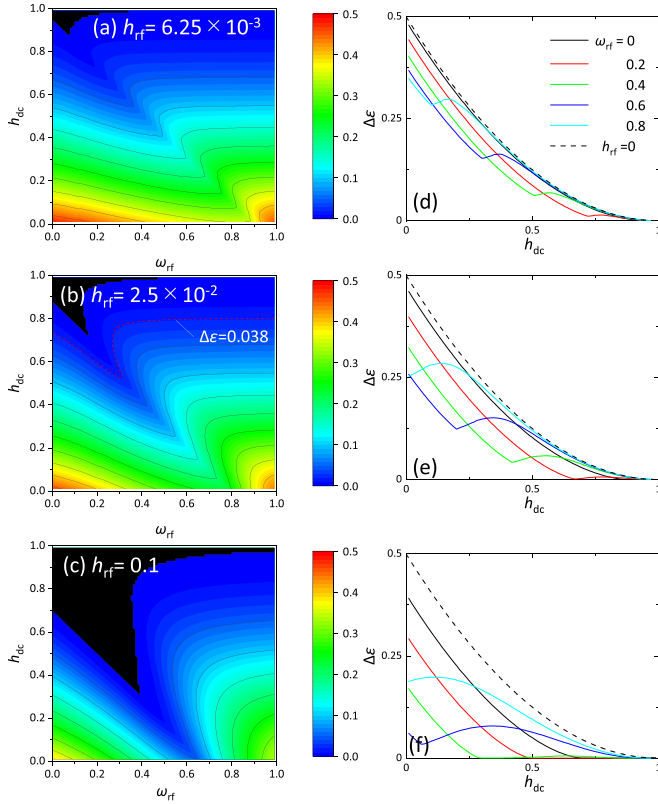


FIG. 5. (a)–(c) Contour map of the effective energy barrier height  $\Delta\varepsilon$  as functions of microwave field frequency  $\omega_{rf}$  and dc applied field  $h_{dc}$  for microwave field amplitude (a)  $h_{rf} = 6.25 \times 10^{-3}$ , (b)  $2.5 \times 10^{-2}$ , and (c) 0.1. (d)–(f) The profiles of the effective energy barrier height  $\Delta\varepsilon$  with microwave field frequency of  $\omega_{rf} = 0$ –0.8 as functions of dc applied field  $h_{dc}$  for microwave field amplitude (d)  $h_{rf} = 6.25 \times 10^{-3}$ , (e)  $2.5 \times 10^{-2}$ , and (f) 0.1. The profile without microwave field is plotted as dashed lines for comparison.

presented. The profile for without a microwave field is also plotted as a dashed line for comparison. The distance between lines increases with increasing  $h_{rf}$ , corresponding to the result that  $\omega_{rf}$  dependence on  $\Delta\varepsilon$  is enhanced by increasing  $h_{rf}$ . For  $\omega_{rf} < \omega_c(0)$ ,  $\Delta\varepsilon$  monotonically decreases with increasing  $h_{dc}$  and reaches zero, at which point irreversible switching occurs deterministically. On the contrary, for  $\omega_{rf} > \omega_c(0)$ , the  $\Delta\varepsilon$  profile becomes nonmonotonic and a dip along with a bump appears. The location of the dip corresponds to the boundary between  $(sr|sd|s)_{l\_min}$  and  $(sr|sd|s)_{max}$ , showing a sharp transition of energy profile at the boundary. The value of  $\Delta\varepsilon$  is getting closer to that for  $h_{rf} = 0$  after passing the bump, corresponding to the fact that magnetization cannot be effectively excited if the microwave field frequency is too high.

In Fig. 6(a),  $\omega_c(\Delta\varepsilon)$  is plotted as a function of  $\Delta\varepsilon$  for  $h_{rf} = 6.25 \times 10^{-3}$ –0.1. The number of points is less for higher  $h_{rf}$ , because  $\omega_c$  for higher  $\Delta\varepsilon$  cannot be defined in the calculated dc field range,  $h_{dc} > 0$ .  $\omega_c(\Delta\varepsilon)$  rapidly increases with  $\Delta\varepsilon$  for all  $h_{rf}$ . The difference of  $\omega_c(\Delta\varepsilon)$  between the curves with different  $h_{rf}$  is almost constant in the whole range, showing that the change in  $\omega_c(\Delta\varepsilon)$  by  $\Delta\varepsilon$  is independent of  $h_{rf}$ . We define two assistance effects  $\Delta h_{dc}^{rf}(\Delta\varepsilon)$  and  $\Delta h_{dc}^{\omega}(\Delta\varepsilon)$ . In Fig. 6(e),

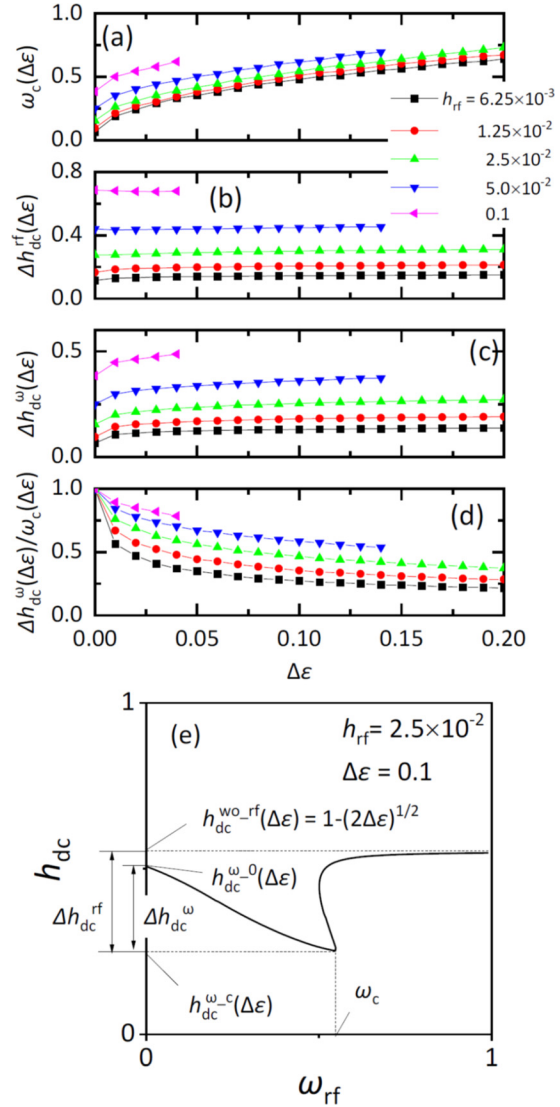


FIG. 6. (a) Critical frequency  $\Delta\omega_c(\Delta\varepsilon)$ . (b) Assistance effect from zero microwave field  $\Delta h_{dc}^{rf}(\Delta\varepsilon)$ . (c) Assistance effect from zero microwave frequency  $\Delta h_{dc}^{\omega}(\Delta\varepsilon)$ . (d) The ratio  $\Delta h_{dc}^{\omega}(\Delta\varepsilon)/\omega_c(\Delta\varepsilon)$  as functions of the effective energy barrier height  $\Delta\varepsilon$  for  $h_{rf} = 6.25 \times 10^{-3}$ –0.1, and (e) definitions of the assistance effects  $\Delta h_{dc}^{rf}(\Delta\varepsilon)$  and  $\Delta h_{dc}^{\omega}(\Delta\varepsilon)$ .

the definitions for  $\Delta h_{dc}^{rf}(\Delta\varepsilon)$  and  $\Delta h_{dc}^{\omega}(\Delta\varepsilon)$  are given using the contour line of the effective energy profile for  $h_{rf} = 2.5 \times 10^{-2}$  and  $\Delta\varepsilon = 0.1$ . The symbols  $\Delta h_{dc}^{wo\_rf}(\Delta\varepsilon)$ ,  $\Delta h_{dc}^{\omega\_0}(\Delta\varepsilon)$ , and  $\Delta h_{dc}^{\omega\_c}(\Delta\varepsilon)$  express the value of  $h_{dc}$  for zero microwave field, with a microwave field of  $\omega = 0$ , and with a microwave field of  $\omega = \omega_c$ , for constant  $\Delta\varepsilon$ .  $\Delta h_{dc}^{rf}(\Delta\varepsilon)$  is given by  $1 - (2\Delta\varepsilon)^{1/2}$ , since  $\Delta\varepsilon$  is given by  $(1 - h_{dc})^2/2$  for the case without a microwave field.  $\Delta h_{dc}^{rf}(\Delta\varepsilon)$  and  $\Delta h_{dc}^{\omega}(\Delta\varepsilon)$  are defined as  $h_{dc}^{wo\_rf}(\Delta\varepsilon) - h_{dc}^{\omega\_c}(\Delta\varepsilon)$  and  $h_{dc}^{\omega\_0}(\Delta\varepsilon) - \Delta h_{dc}^{\omega\_c}(\Delta\varepsilon)$ , respectively.  $\Delta h_{dc}^{rf}(\Delta\varepsilon)$  gives the assistance effect by application of microwave fields from zero microwave field, while  $\Delta h_{dc}^{\omega}(\Delta\varepsilon)$  corresponds to the assistance effect by increasing microwave frequency from zero to  $\omega_c$ . In Figs. 6(b) and 6(c),  $\Delta h_{dc}^{rf}(\Delta\varepsilon)$  and  $\Delta h_{dc}^{\omega}(\Delta\varepsilon)$  are plotted as functions of  $\Delta\varepsilon$  for  $h_{rf} = 6.25 \times 10^{-3}$ –0.1.  $\Delta h_{dc}^{rf}(\Delta\varepsilon)$  is almost constant for all

$h_{rf}$ , indicating that the maximum assistance effect is independent of  $\Delta\varepsilon$  and determined only by  $h_{rf}$ . On the contrary,  $\Delta h_{dc}^{\omega}(\Delta\varepsilon)$  shows a sharp increase in small  $\Delta\varepsilon$  range, but the change becomes very gradual for  $\Delta\varepsilon > 0.02$ . In Fig. 6(d), the ratio  $\Delta h_{dc}^{\omega}(\Delta\varepsilon)/\omega_c(\Delta\varepsilon)$  is plotted as a function of  $\Delta\varepsilon$  for  $h_{rf} = 6.25 \times 10^{-3} - 0.1$ .  $\Delta h_{dc}^{\omega}(\Delta\varepsilon)/\omega_c(\Delta\varepsilon)$  corresponds to the average slope of the frequency dependence of the switching field below  $\omega_c(\Delta\varepsilon)$ , although the contours are not exactly linear as shown in Fig. 5. At  $\Delta\varepsilon = 0$ ,  $\Delta h_{dc}^{\omega}(\Delta\varepsilon)/\omega_c(\Delta\varepsilon) \sim 1$  for all  $h_{rf}$ , which is in good agreement with previous theories at zero temperature. However, with finite values of  $\Delta\varepsilon$ ,  $\Delta h_{dc}^{\omega}(\Delta\varepsilon)/\omega_c(\Delta\varepsilon)$  rapidly decreases with  $\Delta\varepsilon$ . The value of  $\Delta h_{dc}^{\omega}(\Delta\varepsilon)/\omega_c(\Delta\varepsilon)$  strongly depends on  $h_{rf}$  and increases with  $h_{rf}$ . Those results in Fig. 6 give interesting and important predictions about the microwave-assisted switching in the presence of thermal activation: (i) The maximum assistance effect is independent of  $\Delta\varepsilon$  while  $\omega_c(\Delta\varepsilon)$  drastically increases with  $\Delta\varepsilon$ . (ii) The slope of the frequency dependence of the switching field increases with  $h_{rf}$ , but is always more gradual than the values predicted by theories at zero temperature.

The granular media used in this work have the stability factor  $E_0 = 110 k_B T$ . By assuming the Néel-Arrhenius law with the attempt frequency of  $f_0 = 10^{10} \text{ s}^{-1}$ , the relation between  $E_0$  and the relaxation time  $\tau$  is given as  $\tau = f_0^{-1} \exp(-2E_0 \Delta\varepsilon)$ , and  $\Delta\varepsilon = 0.02$  and  $0.125$  gives  $\tau = 8.2 \times 10^{-9}$  and  $88 \text{ s}$ , respectively. The results above indicate that the switching behavior is strongly modified by thermal activation even at  $\Delta\varepsilon = 0.02$ . It suggests that the influence of thermal activation has to be seriously considered in granular media, even in the nanosecond timescale. On the contrary, it has been reported that nanodots have high stability factors; for example,  $E_0 \sim 500 k_B T$  [14]. In this case,  $\Delta\varepsilon = 0.02$  corresponds to  $\tau = 4.9 \times 10^{-2} \text{ s}$ , so that it is expected that most of the previous experiments with a pulsed microwave field have been carried out under the condition  $\Delta\varepsilon < 0.02$ . In that range, the effect of thermal activation is limited, in particular, the case for large  $h_{rf}$ .

### III. LLG MICROMAGNETICS SIMULATION

We have performed numerical simulations based on the LLG equation using open-source micromagnetics software MUMAX3 [30]. In the analytical calculation discussed above, the effective energy  $\varepsilon$  is evaluated by calculating line integrals along the contour of the potential energy. The calculation procedure corresponds to the quasistatic magnetization reversal process, which might be different from the behavior in the nanosecond timescale. Here we employed a system of an array of isolated 256 single spins with uniaxial anisotropy. The volume  $v$  of each spin was set to  $v = 8 \times 8 \times 8 \text{ nm}^3$ . Dipole and exchange interaction between spins were set to zero in the calculation to evaluate the behavior of the isolated spins. The saturation magnetization and the uniaxial anisotropy constant were set to  $M_s = 600 \text{ kA/m}$  and  $K_u = 6 \times 10^5 \text{ J/m}^3$ , respectively, corresponding to the anisotropy field  $\mu_0 H_k = 2 \text{ T}$ . The Gilbert damping constant  $\alpha$  and the gyromagnetic ratio  $\gamma$  were set to  $0.05$  and  $1.94 \times 10^{11} \text{ rad s}^{-1} \text{ T}^{-1}$ , respectively. The thermal activation effect on magnetization switching behavior was evaluated by changing the system temperature while the

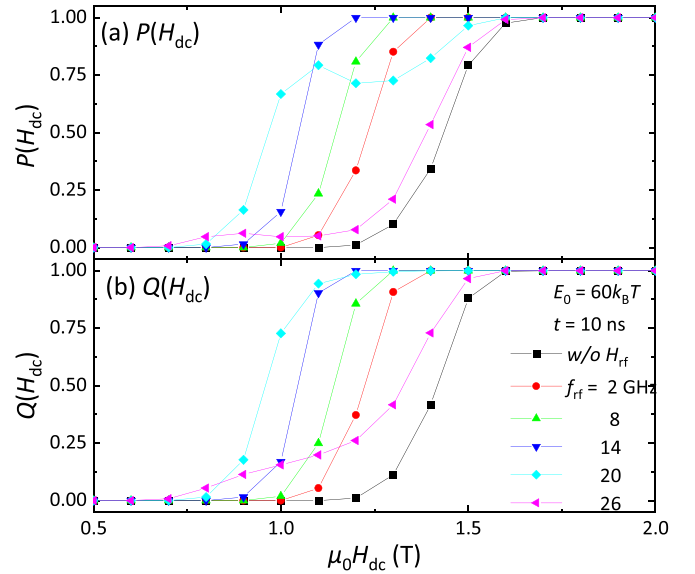


FIG. 7. (a) Switching probability under fixed dc field  $P(H_{dc})$  and (b) switching field under swept field  $Q(H_{dc})$  of an array of 256 isolated single spins as functions of dc field  $H_{dc}$  calculated with a microwave field of  $f_{rf} = 2-26 \text{ GHz}$  and without microwave field. Calculation time  $t_{\text{calc}} = 10 \text{ ns}$  and energy barrier height at zero field  $E_0 = 60 k_B T$  are employed for all calculation.

volume of the spins was fixed. In the calculation, the effect of temperature is introduced as the random fluctuating field [30]. The temperature is given as  $T = K_u v / (k_B E_0) = 2.226 \times 10^4 / E_0$ , where  $E_0$  is the energy barrier height at zero field given in units of  $k_B T$ . The particle volume was set to satisfy the condition  $E_0 = 100 k_B T$  at  $270 \text{ K}$  and the temperature range employed in this work corresponds to  $0.27-1350 \text{ K}$ . In the calculation, the values of  $M_s$  and  $K_u$  were treated as temperature-independent parameters. At the initial state, the magnetization was set to the  $-z$  direction. The dc field  $\mathbf{H}_{dc}$  was applied along the  $+z$  direction as a pulse of  $10 \text{ ns}$  in duration. The microwave field  $\mathbf{H}_{rf}$  was applied as a circularly polarized field in the  $x$ - $y$  plane with amplitude  $H_{rf}$  and frequency  $f_{rf}$ . The switching probability  $P(H_{dc})$  was evaluated as a function of time  $t_{\text{calc}}$  at fixed  $H_{dc}$  and  $H_{rf}$  instead of sweeping  $H_{dc}$ , to compare numerical simulation results with the energy barrier height  $\Delta\varepsilon$ . In Fig. 7(a), calculated switching probability  $P(H_{dc})$  for  $t_{\text{calc}} = 10 \text{ ns}$  is plotted as a function of  $\mu_0 H_{dc}$  for without a microwave field and with a microwave field of  $f_{rf} = 2-26 \text{ GHz}$ . The field step  $\mu_0 \Delta H_{dc}$  is set to be  $0.1 \text{ T}$ . The microwave amplitude  $\mu_0 H_{rf}$  is  $50 \text{ mT}$  and the system temperature was set to satisfy the relation  $E_0 = K_u v = 60 k_B T$ . For  $f_{rf} \leq 14 \text{ GHz}$ , the switching probability increases with  $H_{dc}$  and  $f_{rf}$ , indicating that the microwave field effectively assists magnetization switching. On the contrary, the switching probability for  $f_{rf} = 20 \text{ GHz}$  shows a small bump at  $\mu_0 H_{dc} = 1.1 \text{ T}$ , indicating that the energy barrier height  $\Delta\varepsilon$  has nonmonotonic  $H_{dc}$  dependence at  $f_{rf} = 20 \text{ GHz}$ . This behavior is in good agreement with the profile of  $\Delta\varepsilon$  along  $h_{dc}$  above the critical frequency  $\omega_c(\Delta\varepsilon)$  shown in Figs. 5(d)-5(f). By increasing  $f_{rf}$  further to  $26 \text{ GHz}$ ,  $P(H_{dc})$  shows a small value of about  $0.1$  in the wide range of  $\mu_0 H_{dc} = 0.8-1.2 \text{ T}$ . The behavior corresponds to the flat  $\Delta\varepsilon$

profile around the bump, resulting in the switching probability being insensitive to  $H_{dc}$ . In Fig. 5(b), the contour line for  $\Delta\varepsilon = 0.038$ , which gives the relaxation time of about 10 ns for  $E_0 = 60 k_B T$ , is indicated by the red dashed line. On the contour line, the critical frequency  $\omega_c(\Delta\varepsilon = 0.038)$  and  $h_{dc}$  at  $\omega_c(\Delta\varepsilon = 0.038)$  are given as 0.31 and 0.55, respectively. By multiplying those normalized values by  $\gamma H_k$  and  $H_k$ , respectively, the critical frequency  $f_c$  and the minimum  $\mu_0 H_c$  are obtained to be about 19 GHz and 1.1 T for  $t_{calc} = 10$  ns for  $E_0 = 60 k_B T$ . Those values are reasonable compared with the numerical simulation results shown in Fig. 7(a), indicating that the switching probability shows a critical behavior for  $f_{rf} = 20$  GHz and around  $\mu_0 h_{dc} = 1.1$  T. The switching probability in the swept field  $Q(H_{dc})$  was calculated to evaluate the magnetization curve in the swept field by using the following formula,

$$Q(H_{dc}) = 1 - [1 - Q(H_{dc} - \Delta H_{dc})][1 - P(H_{dc})], \quad (6)$$

where  $\mu_0 \Delta H_{dc}$  is the field step of 0.1 T. Figure 7(b) shows calculated value  $Q(H_{dc})$  as a function of  $\mu_0 H_{dc}$  using the switching probability  $P(H_{dc})$  shown in Fig. 7(a). The calculated curves shift toward smaller  $H_{dc}$  for  $f_{rf} \leq 20$  GHz without significant change of their slopes. On the contrary, the curve for  $f_{rf} = 26$  GHz has an entirely different shape with a gradual slope in the field range of  $\mu_0 H_{dc} \leq 1.3$  T. This gradual slope reflects that the switching probability is insensitive to  $H_{dc}$ , as shown in Fig. 7(a).

In Fig. 8(a), coercivity evaluated from  $Q(H_{dc})$  curves is plotted as a function of microwave frequency  $f_{rf}$  for  $\mu_0 H_{rf} = 12.5$ –100 mT. The result for the linearly polarized (LP) microwave field of  $\mu_0 H_{rf} = 200$  mT is also plotted for comparison. The stability factor was set to  $E_0 = 60 k_B T$ . The plotted points at  $f_{rf} = 0$  are the results without a microwave field. The dashed line indicates the contour line of  $\Delta\varepsilon = 0.038$  for each  $H_{rf}$  calculated by the analytical calculation in the previous section. The numerical simulation results are in good agreement with the analytical calculation, particularly for large  $H_{rf}$ . The difference between the linearly and circularly polarized fields is insignificant, although the assistance effect by the linearly polarized field is larger in the low-frequency region. The deviation in the low-frequency region can be explained by the fact that the clockwise component cannot be neglected entirely because magnetization can follow the microwave field in the frequency range. For smaller  $H_{rf}$ , the assistance effect is smaller than that expected by the analytical calculation, especially around the critical frequency. Such a discrepancy suggests that the effect of the microwave field might be overestimated for smaller  $H_{rf}$  in the analytical calculation. In Fig. 8(b), coercivity for  $E_0 = 20$ – $1 \times 10^5 k_B T$  is plotted as a function of microwave frequency  $f_{rf}$  for  $\mu_0 H_{rf} = 50$  mT. The dashed lines indicate the contour lines for  $\Delta\varepsilon = 0.114$ – $0.0114$ , which corresponds to  $E_0 = 20$ – $200 k_B T$ . The contour line for zero temperature is plotted instead of for  $\Delta\varepsilon = 2.28 \times 10^{-5}$  corresponding to  $E_0 = 1 \times 10^5 k_B T$ , which requires much higher accuracy than our calculation. All curves are in good agreement with the analytical calculation, for both the switching field and the critical frequency. The slope of the frequency dependence becomes gradual by decreasing  $E_0$ , while the critical frequency becomes higher. The maximum

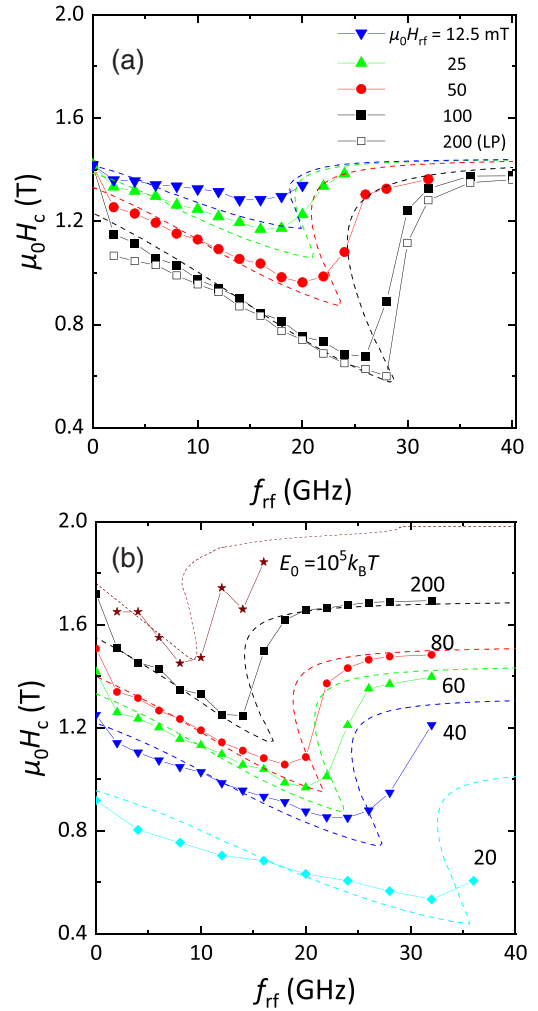


FIG. 8. (a) Numerically simulated coercivity as a function of microwave frequency  $f_{rf}$  for  $E_0 = 60 k_B T$ . Microwave field amplitude is  $\mu_0 H_{rf} = 12.5$ –100 mT for a circularly polarized field and  $\mu_0 H_{rf} = 200$  mT for a linearly polarized field. (b) Numerically calculated coercivity as a function of  $f_{rf}$  for  $\mu_0 H_{rf} = 50$  mT and  $E_0 = 20$ – $10^5 k_B T$ . The dashed lines in the figures show contour lines of energy barrier height  $\Delta\varepsilon$  for corresponding conditions.

change of coercivity becomes slightly larger by increasing  $E_0$ . Note that the critical frequency becomes unclear by decreasing  $E_0$ .

#### IV. MICROWAVE-ASSISTED SWITCHING EXPERIMENTS ON CoCrPt-SiO<sub>2</sub> GRANULAR MEDIA

##### A. Microwave-assisted switching experiment

In this section, we present experimental results on CoCrPt-SiO<sub>2</sub> granular media. The device employed in this paper is identical to the one used in the previous work [27]. A 15 nm thick CoCrPt-SiO<sub>2</sub> granular medium with a composition of Co<sub>72</sub>Pt<sub>20</sub>Cr<sub>8</sub>-30 vol % SiO<sub>2</sub> was deposited with underlayers by dc and rf magnetron sputtering on a shorted coplanar waveguide (CPW) fabricated on a nondoped Si substrate. The thickness and the width of the signal line of the CPW are 100 nm and 1  $\mu\text{m}$ , respectively. The deposited granular medium was patterned into rectangular shaped bars



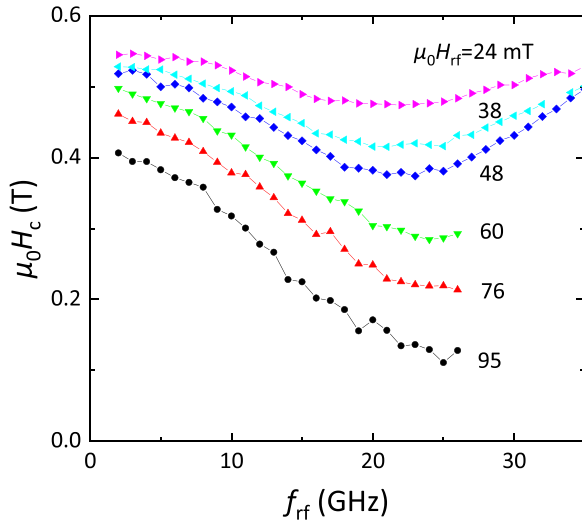


FIG. 9. Coercivity of CoCrPt-SiO<sub>2</sub> granular media as a function of microwave frequency  $f_{rf}$  with microwave field amplitude  $\mu_0 H_{rf} = 24$ –95 mT.

of  $1 \times 3 \mu\text{m}^2$ , and the underlayers were patterned into a cross-shaped electrode for anomalous Hall effect (AHE) measurement. More detailed device structures are reported elsewhere [25]. The saturation magnetization  $M_s$  and the uniaxial anisotropy constant  $K_u$  of the continuous film were evaluated to be 660 kA/m and  $6.2 \times 10^5 \text{ J/m}^3$ , respectively. The anisotropy constant corresponds to the anisotropy field  $\mu_0 H_k = 1.88 \text{ T}$  with the easy axis along the film normal. The stability factor  $E_0$  was evaluated to be  $110 k_B T$  by measuring the time dependence of coercivity using a pulsed magnet. AHE measurements were carried out to measure the magnetization curves of the media in a dc field along the film normal. The typical measurement time for one magnetization curve was 480 s with a field range of  $\pm 1.5 \text{ T}$ . The microwave field was generated by applying microwave current to the CPWs using a signal generator (Keysight N5183A). We employed two amplifiers with different frequency ranges and maximum amplitudes (Keysight 83051A and 83020A). The obtained maximum microwave field amplitude was 48 and 95 mT for up to  $f_{rf} = 35$  and 26 GHz, respectively.

Figure 9 shows the microwave frequency  $f_{rf}$  dependence of coercivity  $H_c$  of the CoCrPt-SiO<sub>2</sub> granular media measured with a linearly polarized microwave field with amplitude  $\mu_0 H_{rf} = 24$ –95 mT. Microwave fields were applied as continuous waves during the magnetization curve measurement. The measured frequency range for  $\mu_0 H_{rf} > 48 \text{ mT}$  is limited to  $f_{rf} \leq 26 \text{ GHz}$  due to the frequency range of the microwave amplifiers. The assistance effect increases with increasing  $H_{rf}$ . Coercivity monotonically decreases with increase in microwave frequency for  $f_{rf} < 20 \text{ GHz}$ , then turns to a gradual increase with increasing  $f_{rf}$  showing its minimum in the range  $f_{rf} = 20$ –25 GHz, depending on  $H_{rf}$ . Here we define the frequency at which  $H_c$  become minimum as the experimental critical frequency  $f_c^{\text{expt.}}$ . The value of  $f_c^{\text{expt.}}$  slightly increases with increasing  $H_{rf}$ . The slope of the frequency dependence of coercivity in the low-frequency

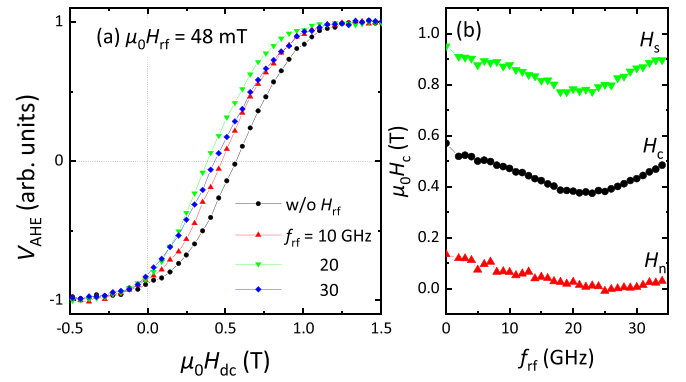


FIG. 10. (a) Anomalous Hall effect curves of CoCrPt-SiO<sub>2</sub> granular media measured without and with a microwave field of  $f_{rf} = 10$ –30 GHz. (b) Nucleation field  $\mu_0 H_n$ , coercivity  $\mu_0 H_c$ , and saturation field  $\mu_0 H_s$  of CoCrPt-SiO<sub>2</sub> granular media as functions of microwave frequency  $f_{rf}$ . The microwave field amplitude  $\mu_0 H_{rf} = 48 \text{ mT}$ .

region becomes steeper from  $-4$  to  $-16 \text{ mT/GHz}$  for  $\mu_0 H_{rf} = 24$  to 95 mT, and all those values are still more gradual than  $-2\pi/\gamma$ .

Figure 10(a) shows AHE curves of CoCrPt-SiO<sub>2</sub> granular media measured with a microwave field of  $\mu_0 H_{rf} = 48 \text{ mT}$  and  $f_{rf} = 10$ –30 GHz. The dc field  $H_{dc}$  was swept from negative to positive. An AHE curve measured without microwave field application is plotted for comparison. The slope of the AHE curves is almost unchanged for  $f_{rf} < 20 \text{ GHz}$ , while the coercivity shifts by the microwave assistance effect. However, the slope becomes gradual by increasing  $f_{rf}$  further to 30 GHz because it becomes harder to saturate, although the assistance effect is still effective around coercivity. In Fig. 10(b), the nucleation field  $H_n$ , the coercivity  $H_c$ , and the saturation field  $H_s$  measured for  $\mu_0 H_{rf} = 48 \text{ mT}$  are plotted as functions of  $f_{rf}$ .  $H_n$  and  $H_s$  are defined as the fields at which the normalized AHE voltage reaches  $-0.8$  and  $0.8$ , respectively. All of  $H_n$ ,  $H_c$ , and  $H_s$  show similar microwave frequency dependencies characterized by a linear decrease in the low-frequency range and broad minimum. However, the frequencies at which those values become minimum are slightly different.  $H_n$  shows the minimum at the highest frequency of 25 GHz and is followed by  $H_c$  and  $H_s$  of 22 and 19 GHz, respectively. Such difference of frequency dependence appears as the gradual slope of the magnetization curve for  $f_{rf} = 30 \text{ GHz}$  shown in Fig. 10(a). The result indicates that the effectiveness of microwave assistance is determined not only by the condition of the microwave field but also by the value of the applied dc field, particularly for high  $f_{rf}$ .

## B. Comparison with calculation results

The stability factor  $E_0 = 110 k_B T$  and the effective energy barrier height  $\Delta\varepsilon = 0.125$  give the relaxation time  $\tau = 88 \text{ s}$ , which is of the same order as the measurement time in this work. By multiplying the values of  $\omega_c(\Delta\varepsilon = 0.125)$  and  $h_{dc}$  at  $\omega_c(\Delta\varepsilon = 0.125)$  with  $\gamma H_k$  and  $H_k$ , respectively, these normalized values can be converted to the expected value of critical

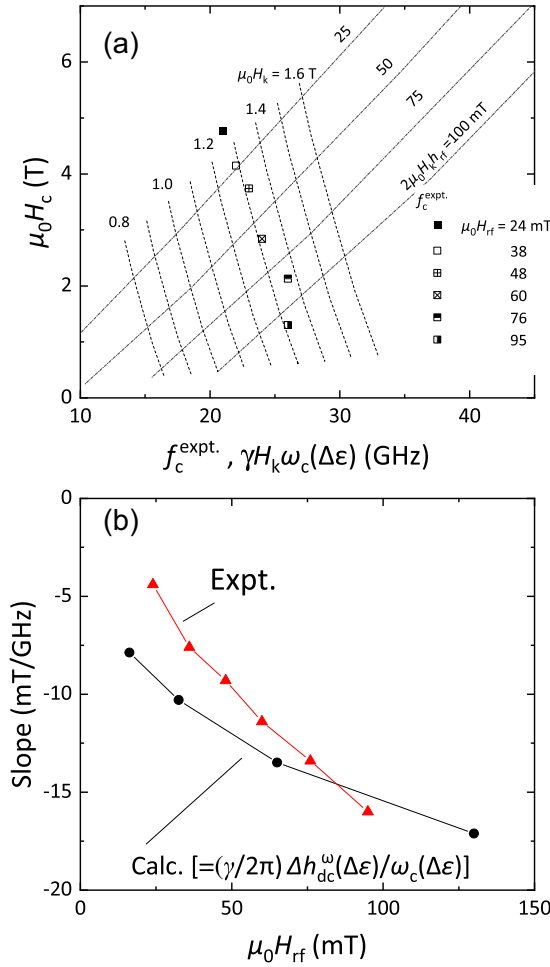


FIG. 11. (a) Coercivity  $\mu_0 H_c$  of CoCrPt-SiO<sub>2</sub> granular media as a function of the experimentally observed critical frequency  $f_c^{\text{expt.}}$  for  $\mu_0 H_{\text{rf}} = 24$ –95 mT. The lines indicate the contour lines for the switching field with various anisotropy field  $\mu_0 H_k$  and microwave field amplitude  $2\mu_0 H_k h_{\text{rf}}$  evaluated by the energy barrier height calculation. (b) Average slope of frequency dependence of coercivity of CoCrPt-SiO<sub>2</sub> granular media as a function of microwave field amplitude  $H_{\text{rf}}$ . Average slope evaluated by the analytical calculation  $[= \Delta h_{\text{dc}}^{\omega}(\Delta\varepsilon)/\omega_c(\Delta\varepsilon)]$  for  $\Delta\varepsilon = 0.125$  is also plotted. The calculated value is multiplied by  $(\gamma/2\pi)$ .

frequency and coercivity in experiments. In Fig. 11(a), coercivity  $H_c$  at the experimentally observed critical frequency  $f_c^{\text{expt.}}$  of CoCrPt-SiO<sub>2</sub> granular media is plotted as a function of  $f_c^{\text{expt.}}$ . The symbols represent the microwave field amplitude  $\mu_0 H_{\text{rf}} = 24$ –95 mT. The contour lines in Fig. 11(a) are calculated by using the values of  $H_k h_{\text{dc}}$  and  $\gamma H_k \omega_c(\Delta\varepsilon)$  for various anisotropy field  $H_k$  and microwave field amplitude  $2H_k h_{\text{rf}}$ . It should be noted that the microwave field amplitude for the calculation is doubled to compensate for the difference between circularly and linearly polarized fields. All points for experiments are located along the contour lines for the anisotropy field  $\mu_0 H_k = 1.3$  T, and the value of  $H_{\text{rf}}$  shows only slight differences from the contour lines. In our previous work, the autocorrelation length of magnetization reversal under microwave excitation has been evaluated to be 150 nm by X-ray magnetic circular dichroism (XMCD) microscopy

measurement [25]. Assuming that the reversal unit is an oblate spheroid of 15 nm in thickness and 150 nm in diameter, the demagnetization factor along the in-plane direction  $N_x$  and along the film normal  $N_z$  are evaluated to be 0.07 and 0.86, respectively. Since the demagnetization field from outside of the reversal unit is canceled at the coercivity, the effective anisotropy field  $H_k^{\text{eff}} = H_k - 4\pi(N_z - N_x)M_s$  can be deduced to be  $\mu_0 H_k^{\text{eff}} = 1.22$  T by substituting  $\mu_0 H_k = 1.88$  T and  $M_s = 660$  kA/m. This value is in good agreement with the value of the anisotropy field of 1.3 T evaluated in Fig. 11(a). In Fig. 11(b), the average slope of frequency dependence of coercivity of the CoCrPt-SiO<sub>2</sub> granular media below the critical frequency is plotted as a function of  $H_{\text{rf}}$ . The average slope  $\Delta h_{\text{dc}}^{\omega}(\Delta\varepsilon)/\omega_c(\Delta\varepsilon)$  for  $\Delta\varepsilon = 0.125$  by the analytical calculation, which is shown in Fig. 6(d), multiplied by  $\gamma/2\pi$  is also plotted as a function of  $H_{\text{rf}} = 2H_k h_{\text{rf}}$ . Here, we employed  $\mu_0 H_k = 1.3$  T and the factor 2 is required to compensate for the difference of circularly and linearly polarized fields. The value of the slopes in the experiments increases with increasing  $H_{\text{rf}}$ . The value of the slope reaches  $-16$  for  $\mu_0 H_{\text{rf}} = 95$  mT, but it remains about half of  $-2\pi/\gamma (= -0.32)$ , which is the expected value at zero temperature. The calculated slope also shows a similar value and  $H_{\text{rf}}$  dependence, indicating that the gradual and microwave amplitude dependent slope in granular media can be explained quantitatively by considering the thermal activation effect. The experimental data tend to be slightly larger for the small  $H_{\text{rf}}$  region. The results of numerical simulation also show more gradual slopes compared with that of the analytical calculation as shown in Fig. 8(a), suggesting that the effective energy calculation procedure might overestimate the assistance effect. The gradual slope of the magnetization curve found above the critical frequency can also be explained by considering the thermal activation process. As shown in the contour map in Figs. 5(a)–5(c), the effective energy becomes almost insensitive to  $\omega_{\text{rf}}$  and  $h_{\text{dc}}$  just above critical frequency. Therefore, the switching probability takes small constant values as observed in the numerical calculation, resulting in the gradual slope of the magnetization curve lying between the nucleation field at the critical frequency and the saturation field without a microwave field.

## V. CONCLUSIONS

We have studied, theoretically and experimentally, microwave-assisted switching in the presence of thermal activation. The effective energy barrier height  $\Delta\varepsilon$  has been calculated based on the LLG equation in the rotating frame as functions of dc field  $h_{\text{dc}}$  and microwave frequency  $\omega_c$  for various microwave field amplitudes  $h_{\text{rf}}$ . Analysis of the effective energy barrier height  $\Delta\varepsilon$  has revealed that the microwave frequency and amplitude dependences are strongly modified by thermal activation. Although the presence of thermal activation increases the critical frequency, the maximum assistance effect is insensitive to the energy barrier height  $\Delta\varepsilon$  and mainly determined only by microwave field amplitude. Numerical simulation based on the LLG equation has revealed that the analytical calculation reproduces the switching field under a microwave field, although it might overestimate the assistance effect in the case where the microwave field amplitude is below a few percent. Experimental results on

CoCrPt-SiO<sub>2</sub> granular media showed characteristic behavior, namely, the microwave field amplitude dependence of slope of frequency dependences, the high critical frequency, and the change of the slope of magnetization curve at high frequency. All those behaviors are well explained by considering the profile of the effective energy barrier height, indicating that thermal activation plays an essential role in microwave-assisted switching in granular media. The coercivity and critical frequency can be quantitatively explained successfully by considering the effective anisotropy field of the magnetization reversal unit. Those results indicate the importance

of evaluating the effect of the thermal activation process on microwave-assisted switching for designing future practical devices.

#### ACKNOWLEDGMENTS

This work was partly supported by JSPS KAKENHI (Grants No. 17K05028 and No. 17H03227), Network Joint Research Center for Materials and Devices: Dynamic Alliance for Open Innovation Bridging Human, Environment and Materials from MEXT, and ASRC.

- 
- [1] J.-G. Zhu, X. Zhu, and Y. Tang, *IEEE Trans. Magn.* **44**, 125 (2008).
- [2] S. Batra and W. Scholz, *IEEE Trans. Magn.* **44**, 3392 (2008).
- [3] G. Winkler, D. Suess, J. Lee, J. Fidler, M. A. Bashir, J. Dean, A. Goncharov, G. Hrkac, S. Bance, and T. Schrefl, *Appl. Phys. Lett.* **94**, 232501 (2009).
- [4] Y. Shiroishi, K. Fukuda, I. Tagawa, H. Iwasaki, S. Takenoiri, H. Tanaka, H. Mutoh, and N. Yoshikawa, *IEEE Trans. Magn.* **45**, 3816 (2009).
- [5] G. Bertotti, I. D. Mayergoyz, C. Serpico, M. D'Aquino, and R. Bonin, *J. Appl. Phys.* **105**, 07B712 (2009).
- [6] S. Okamoto, N. Kikuchi, and O. Kitakami, *Appl. Phys. Lett.* **93**, 102506 (2008).
- [7] S. Okamoto, M. Igarashi, N. Kikuchi, and O. Kitakami, *J. Appl. Phys.* **107**, 123914 (2010).
- [8] T. Taniguchi, *Phys. Rev. B* **90**, 024424 (2014).
- [9] H. Suto, K. Kudo, T. Nagasawa, T. Kanao, K. Mizushima, R. Sato, S. Okamoto, N. Kikuchi, and O. Kitakami, *Phys. Rev. B* **91**, 094401 (2015).
- [10] H. Arai and H. Imamura, *Jpn. J. Appl. Phys.* **55**, 028002 (2016).
- [11] K. Rivkin, M. Benakli, N. Tabat, and H. Yin, *J. Appl. Phys.* **115**, 214312 (2014).
- [12] S. Okamoto, N. Kikuchi, M. Furuta, O. Kitakami, and T. Shimatsu, *J. Phys. D: Appl. Phys.* **48**, 353001 (2015).
- [13] C. Thirion, W. Wernsdorfer, and D. Maily, *Nat. Mater.* **2**, 524 (2003).
- [14] S. Okamoto, N. Kikuchi, M. Furuta, O. Kitakami, and T. Shimatsu, *Phys. Rev. Lett.* **109**, 237209 (2012).
- [15] M. Furuta, S. Okamoto, N. Kikuchi, O. Kitakami, and T. Shimatsu, *Appl. Phys. Express* **6**, 053006 (2013).
- [16] M. Furuta, S. Okamoto, N. Kikuchi, O. Kitakami, and T. Shimatsu, *J. Appl. Phys.* **115**, 133914 (2014).
- [17] H. Suto, T. Kanao, T. Nagasawa, K. Mizushima, and R. Sato, *Sci. Rep.* **7**, 13804 (2017).
- [18] H. Suto, T. Kanao, T. Nagasawa, K. Mizushima, and R. Sato, *Phys. Rev. Appl.* **9**, 54011 (2018).
- [19] C. T. Boone, J. A. Katine, E. E. Marinero, S. Pisana, and B. D. Terris, *J. Appl. Phys.* **111**, 07B907 (2012).
- [20] C. Boone, J. A. Katine, E. E. Marinero, S. Pisana, and B. D. Terris, *IEEE Magn. Lett.* **3**, 3500104 (2012).
- [21] S. Okamoto, N. Kikuchi, A. Hotta, M. Furuta, O. Kitakami, and T. Shimatsu, *Appl. Phys. Lett.* **103**, 202405 (2013).
- [22] Y. Nakayama, Y. Kusanagi, T. Shimatsu, N. Kikuchi, S. Okamoto, and O. Kitakami, *IEEE Trans. Magn.* **52**, 3201203 (2016).
- [23] Y. Nozaki, N. Ishida, Y. Soeno, and K. Sekiguchi, *J. Appl. Phys.* **112**, 083912 (2012).
- [24] N. Ishida, Y. Soeno, K. Sekiguchi, and Y. Nozaki, *J. Appl. Phys.* **114**, 043915 (2013).
- [25] Y. Nozaki and S. Kasai, *IEEE Trans. Magn.* **52**, 3100207 (2016).
- [26] N. Kikuchi, K. Shimada, T. Shimatsu, S. Okamoto, and O. Kitakami, *Jpn. J. Appl. Phys.* **57**, 09TE02 (2018).
- [27] N. Kikuchi, K. Sato, S. Kikuchi, S. Okamoto, T. Shimatsu, O. Kitakami, H. Osawa, and M. Suzuki, *J. Appl. Phys.* **126**, 083908 (2019).
- [28] T. Taniguchi, Y. Utsumi, and H. Imamura, *Phys. Rev. B* **88**, 214414 (2013).
- [29] G. Bertotti, A. Magni, I. D. Mayergoyz, and C. Serpico, *J. Appl. Phys.* **89**, 6710 (2001).
- [30] A. Vansteenkiste, J. Leliaert, M. Dvornik, M. Helsen, F. Garcia-Sanchez, and B. Van Waeyenberge, *AIP Adv.* **4**, 107133 (2014).